Proceedings of the
Annual Stability Conference
Structural Stability Research Council
St. Louis, Missouri, April 2-5, 2019

On the buckling behavior of thin-walled steel tubes subjected to combinations of axial compression and external lateral pressure

Cilmar Basaglia[1], Dinar Camotim[2], Nuno Silvestre[3]

Abstract
This paper reports the results of a numerical investigation on the buckling behavior of thin-walled steel tubes subjected to combinations of axial compression and external lateral pressure – these results are obtained by means of a GBT-based beam finite element formulation, recently developed by the authors, and also ANSYS shell finite element analyses. After providing a brief overview of the main concepts and procedures involved in performing GBT buckling analyses of circular cylindrical steel shells (such as cylinders/tanks and pipes), a parametric study is presented. It deals with the assessment of the buckling behavior of thin-walled steel tubes (radius-to-thickness ratio below *100*) under various combinations of axial compression and external lateral pressure. In particular, the joint influence of the loading, length-to-radius ratio and radius-to-thickness ratio on the tube critical buckling load and mode shape is investigated.

1. Introduction

The undersea or underground pipelines and jacket offshore platforms used in the petroleum industry are often formed by circular thin-walled steel tubes that are normally acted by combinations of axial compression and external lateral pressure. When such tubes exhibit slender cross-sections they are highly susceptible to the occurrence of local and/or global buckling phenomena, a feature that renders the numerical assessment of their structural behavior and strength a complex task (Teng & Rotter 2004). Various approaches have been used to assess the buckling behavior of circular cylindrical steel shells under hydrostatic external pressure. Probably the most popular of them consists of using the energy method to determine the critical buckling pressure (Arjomandi 2010). On the other hand, an analytical solution to obtain bifurcation/buckling loads of cylindrical tubes under combined external pressure and axial compression, using Donnell's simplified equations, was developed, almost half a century ago, by Krishnamorthy (1974) – however, the major difficulty associated with the development and usage of closed form solution stems from (i) the presence of expressions with various undetermined coefficients and (ii) the mathematical determination of the number of lobes, *i.e.*, circumferential waves associated with the tube buckling mode. The numerical assessment of the structural response of circular cylindrical steel shells under hydrostatic external pressure also constitutes a complex task. Indeed, rigorous numerical analyses can only be performed by resorting to shell finite element models, a time-consuming

[1] FEC, DES, University of Campinas. <cbasaglia@fec.unicamp.br>
[2] CERIS, DECivil, Instituto Superior Técnico, Universidade de Lisboa. <dcamotim@ist.utl.pt>
[3] IDMEC, DEM, Instituto Superior Técnico, Universidade de Lisboa. <nsilvestre@ist.utl.pt>

approach still prohibitive for routine applications (*e.g.*, Ross 2011). Moreover, the differential equation governing the adjacent equilibrium of a shell structure acted by external pressure and axial compression must take into account the follower nature of the lateral pressure, *i.e.*, the fact that it changes direction during the shell deformation, in order to remain always normal to the shell wall (*e.g.*, Paimushin 2008).

A promising alternative approach is the use of Generalized Beam Theory (GBT), a thin-walled prismatic bar theory incorporating genuine plate/shell theory concepts. The authors have recently developed and numerically implemented a GBT formulation specifically aimed at investigating the buckling behavior of circular cylindrical shells subjected to axial compression and external pressure (Basaglia *et al.* 2016) – up to now, this GBT formulation has been validated and applied exclusively in the context of (i) tubes under external pressure alone and (ii) pressure vessels subjected to hydrostatic pressure (*i.e.*, acted by small axial compressive stresses along its length).

In the available literature on shell buckling, the curvature effects are often taken into account through the normalized/dimensionless Batdorf parameter $Z = L^2(1-\upsilon^2)^{1/2} / rt$, where υ is Poisson's ratio and L, r and t are the shell length, radius and thickness, respectively (Batdorf 1947) – the limit case of Z equal to zero corresponds to a flat plate. Basaglia *et al.* (2016) have shown that, when Z is small and the aspect ratio L/r is not too large, the buckling mode shape of shells/tanks under hydrostatic pressure exhibits a large number of circumferential half-waves. A thorough search of the relevant literature showed that very few results are available concerning the buckling behavior of thin-walled steel tubes with radius-to-thickness ratios (r/t) below *100* and subjected to combined axial compression and external pressure (*e.g.*, Galletly & Pemsing 1985) – this is mostly due to the fact that major oil and gas land pipelines have r/t values ranging between *20* and *40* (Kyriakides & Corona 2007). However, there are several results available in the literature dealing with the buckling behavior of cylindrical shells under combined loading and exhibiting geometries characterized by $r/t \geq 100$ and $Z < 4000$ – such geometries are fairly common in chimneys, silos, tanks and many aerospace/mechanical structures. In this context, it is worth noting the works due to Weingarthen & Seide (1965), Tennyson *et al.*, (1978), Yamaki (1984), Shen & Chen (1991), Winterstetter & Schmidt (2002) and Sun *et al.* (2016).

The work presented in this paper aims at contributing to fill the gap identified in the previous paragraph, by performing a parametric study dealing with the assessment of the buckling behavior of thin-walled steel tubes (i) subjected to combination of axial compression and external lateral pressure and (ii) exhibiting geometrical and material properties such that $r/t \leq 100$ and the Z parameter varies from small to large. The determination of the critical bifurcation load/pressure values and corresponding buckling mode shapes is carried out by means of a Generalized Beam Theory specialization that makes it possible to solve a large number of problems in a very short period of time – in this particular case, several combinations of loading, length-to-radius ratio and radius-to-thickness ratio are considered. For validation purposes, some GBT results are compared with values obtained by means of ANSYS shell finite element analyses (SAS 2013). Finally, on the basis of the results gathered, the key parameters governing the buckling behaviors under consideration are identified and discussed.

2. GBT Main Concepts and Procedures

Because the cross-section displacement field is expressed as a linear combination of mechanically meaningful deformation modes, GBT analyses (i) lead to equilibrium equations written in a rather convenient form and (ii) make it possible to perform modal analyses of prismatic thin-walled members, which provide very clear insight on their structural behavior. Figure 1 depicts a prismatic member with

a circular hollow section, having radius r and wall thickness t, and the global coordinate system X, Y, Z. In order to account for the cross-section in-plane deformation effects, it is preferable to consider the local coordinate system x, θ, z, (longitudinal coordinate $x \in [0;L]$, angular coordinate $\theta \in [0;2\pi]$ and thickness coordinate $z \in [-t/2; +t/2]$) – u,v,w are the displacement components in the local coordinate system.

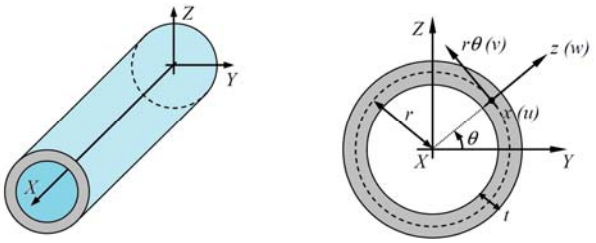

Figure 1: Circular hollow section member and global and local coordinate system and displacement components.

In order to obtain a displacement field representation compatible with the classical beam theory, each displacement component (u, v or w) at any given point of the cross-section mid-surface must be expressed as a combination of orthogonal functions. Therefore, one has

$$u(x,\theta) = u_k(\theta)\phi_{k,x}(x) \qquad v(x,\theta) = v_k(\theta)\phi_k(x) \qquad w(x,\theta) = w_k(\theta)\phi_k(x) \quad , \quad (1)$$

where (i) the summation convention applies to subscript k and (ii) $u_k(\theta)$, $v_k(\theta)$ and $w_k(\theta)$ are functions characterizing deformation mode k (Silvestre 2007). Since the thin-walled member is deemed made of an isotropic elastic material (*e.g.*, constructional steel), the constitutive relation reads

$$\begin{Bmatrix} \sigma_{xx} \\ \sigma_{\theta\theta} \\ \tau_{x\theta} \end{Bmatrix} = \begin{bmatrix} \frac{E}{1-\upsilon^2} & \frac{E\upsilon}{1-\upsilon^2} & 0 \\ \frac{E\upsilon}{1-\upsilon^2} & \frac{E}{1-\upsilon^2} & 0 \\ 0 & 0 & G \end{bmatrix} \begin{Bmatrix} \varepsilon_{xx} \\ \varepsilon_{\theta\theta} \\ \gamma_{x\theta} \end{Bmatrix} \quad , \quad (2)$$

where (i) E, G and υ are Young's modulus, shear modulus and Poisson's ratio and (ii) σ_{ij}, ε_{ij}, γ_{ij} are the plane stress and strain components. The linear and non-linear (^{NL}) kinematic relations adopted satisfy Love-Kirchhoff's assumption and can be expressed, in terms of the mid-plane displacement components (u, v, w), as (Basaglia *et al.* 2016)[4]

$$\varepsilon_{xx} = u_k\phi_{k,xx} - zw_k\phi_{k,xx} \quad (3)$$

$$\varepsilon_{\theta\theta} = \frac{v_{k,\theta} + w_k}{r}\phi_k - z\frac{w_{k,\theta\theta} - v_{k,\theta}}{r^2}\phi_k \quad (4)$$

$$\gamma_{x\theta} = \left(\frac{u_{k,\theta}}{r} + v_k\right)\phi_{k,x} - z\left(\frac{4rw_{k,\theta} - 3rv_k + u_{k,\theta}}{2r^2}\right)\phi_{k,x} \quad (5)$$

$$\varepsilon_{xx}^{NL} = \frac{1}{2}w_k w_i \phi_{k,x}\phi_{i,x} + \frac{1}{8}\left(v_k - \frac{u_{k,\theta}}{r}\right)\left(v_i - \frac{u_{i,\theta}}{r}\right)\phi_{k,x}\phi_{i,x} \quad (6)$$

[4] Since the buckling behavior under torsion is not addressed in this work, the non-linear shear strain component is disregarded.

$$\varepsilon_{\theta\theta}^{NL} = \frac{1}{2}\left(\frac{v_k - w_{k,\theta}}{r}\right)\left(\frac{v_i - w_{i,\theta}}{r}\right)\phi_k\phi_i + \frac{1}{8}\left(v_k - \frac{u_{k,\theta}}{r}\right)\left(v_i - \frac{u_{i,\theta}}{r}\right)\phi_{k,x}\phi_{i,x} \quad . \quad (7)$$

When performing buckling analyses of thin-walled members, such as cylinders and tubes, the application of the Principle of Virtual Work, leading to the member equilibrium equations, reads

$$\delta W_{int} + \delta W_{ext} = \delta W^{L} + \delta W^{NL} + \delta W_{ext} = 0 \quad , \quad (8)$$

where (i) δW_{int} is the work done by the internal forces (pre-buckling stresses) on the virtual strains, which can still subdivided in two additive parts, namely the works done on the strains stemming from linear (δW^{L}) and non-linear (δW^{NL}) terms of the strain-displacement relations, and (ii) δW_{ext} is the (path-dependent) work done by follower external pressure on the cylinder/pipe wall virtual displacements[5].

The work done by the internal forces (pre-buckling stresses) on the virtual strains is given by

$$\delta W_{int} = \delta W^{L} + \delta W^{NL} = \int_L \oint_t \int (\sigma_{xx}\delta\varepsilon_{xx} + \sigma_{\theta\theta}\delta\varepsilon_{\theta\theta} + \tau_{x\theta}\delta\gamma_{x\theta} + \sigma_{xx}^{0}\delta\varepsilon_{xx}^{NL} + \sigma_{\theta\theta}^{0}\delta\varepsilon_{\theta\theta}^{NL})dzrd\theta dx \quad , \quad (9)$$

where (i) L, r and t are the member length, cross-section mid-surface radius and thickness, respectively, and (ii) σ_{xx}^{0} and $\sigma_{\theta\theta}^{0}$ are the pre-buckling longitudinal stresses due to axial compression and hoop stresses (stresses acting along the circumferential direction) caused by the applied external pressure p^0, as illustrated in Figure 2 – the hoop stresses are given by

$$\sigma_{\theta\theta}^{0} = \frac{p^0 r}{t} \quad . \quad (10)$$

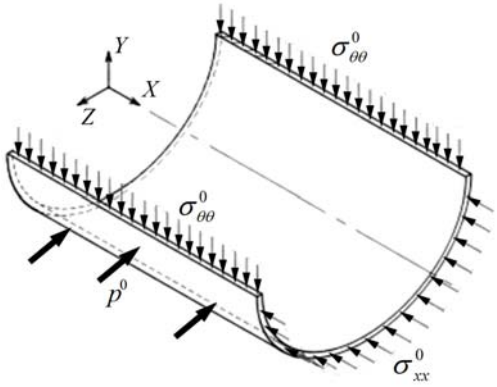

Figure 2: Pre-buckling longitudinal σ_{xx}^{0} and hoop $\sigma_{\theta\theta}^{0}$ stresses.

On account of the above (i) displacement approximations, (ii) constitutive law and (iii) kinematic relations, it is possible to rewrite the works done by the internal forces on the strains due to the linear and non-linear strain-displacement relation terms as

$$\delta W^{L} = \int_L (C_{ik}\phi_{k,xx}\delta\phi_{i,xx} + D_{ik}^{1}\phi_{k,x}\delta\phi_{i,x} + D_{ik}^{2}\phi_k\delta\phi_{i,xx} + D_{ki}^{2}\phi_{k,xx}\delta\phi_i + B_{ik}\phi_k\delta\phi_i)dx \quad (11)$$

[5] Since the shell material behavior is linear elastic, δW_{int} can also be viewed as the first variation of the shell strain energy.

$$\delta W^{NL} = \int_L (X^{\sigma xx}_{jik} \phi_{k,x} \delta\phi_{i,x} + X^{1\sigma\theta\theta}_{jik} \phi_k \delta\phi_i + X^{2\sigma\theta\theta}_{jik} \phi_{k,x} \delta\phi_{i,x}) dx \quad , \quad (12)$$

where the tensors stem from the cross-section integration of displacement components and derivatives – their expressions can be found in Basaglia *et al.* (2016). In the presence of (follower) external lateral pressure, Paimushin (2008) showed that, as long as the rotations are small-to-moderate, the external work is given by the expression

$$\delta W_{ext} = -\int_L \oint_t \int p^0 \left(-w_{,x} \delta u - \frac{w_{,\theta} - v}{r} \delta v \right) dz r d\theta dx \quad (13)$$

or, incorporating the displacement approximations expressed in Eqs. (1), by (Basaglia *et al.* 2016)

$$\delta W_{ext} = \int_L (H^1_{ik} \phi_{k,x} \delta\phi_{i,x} + H^2_{ik} \phi_k \delta\phi_i) dx \quad , \quad (14)$$

where

$$H^1_{ik} = \oint p^0 w_k u_i t r d\theta \quad (15)$$

$$H^2_{ik} = \oint p^0 \left(\frac{w_{k,\theta} - v_k}{r} \right) v_i t r d\theta \quad . \quad (16)$$

2.1 Deformation Modes

The cross-section analysis, performed to obtain the deformation modes and corresponding mechanical properties, comprises a set of sequential operations already described in detail by Schardt (1989), Silvestre (2007) and Basaglia *et al.* (2015). The deformation modes most relevant for the buckling analyses carried out in this paper (*i.e.*, those with significant contributions to the tube buckling mode shapes) consist of (i) a shell-type deformation mode family (originally considered by Schardt 1989) and (ii) an axisymmetric mode (first unveiled by Silvestre 2007). The shell-type modes, based on the assumption of null membrane shear strains and transverse extensions, constitute the core of the GBT analysis of circular hollow section members – the in-plane shapes of the first 14 shell-type modes are depicted in Figure 3. The axisymmetric mode, identified by the label "**a**", involves only in-plane displacements and accounts for the cross-section deformation due to the extension in the circumferential direction – thus, the associated displacement profile is characterized by $u_a=0$, $v_a=0$ and $w_a=1$ (see Fig. 4).

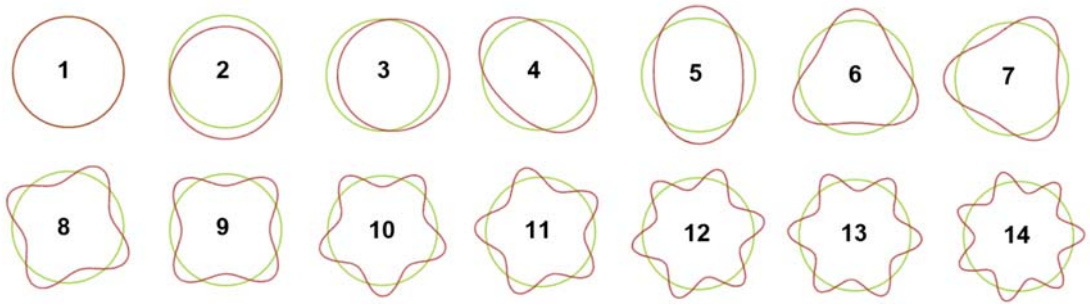

Figure 3: In-plane shapes of the first 14 shell-type deformation modes of a circular hollow cross-section.

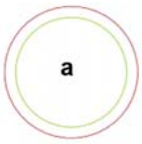

Figure 4: Axisymmetric (**a**) deformation mode of a circular hollow cross-section.

2.2 Beam Finite Element Formulation

After incorporating the cross-section mechanical, geometric and follower pressure properties into the variational equation (see (8)), one is lead to

$$\int_L (C_{ik}\phi_{k,xx}\delta\phi_{i,xx} + D^1_{ik}\phi_{k,x}\delta\phi_{i,x} + D^2_{ik}\phi_k\delta\phi_{i,xx} + D^2_{ki}\phi_{k,xx}\delta\phi_i + B_{ik}\phi_k\delta\phi_i + \\ + X^{\sigma xx}_{jik}\phi_{k,x}\delta\phi_{i,x} + X^{1\sigma\theta\theta}_{jik}\phi_k\delta\phi_i + X^{2\sigma\theta\theta}_{jik}\phi_{k,x}\delta\phi_{i,x} + H^1_{ik}\phi_{k,x}\delta\phi_{i,x} + H^2_{ik}\phi_k\delta\phi_i)dx \quad , \quad (17)$$

a system of equilibrium equations (one per deformation mode) that, together with the member support conditions (written in modal form), defines a one-dimensional eigenvalue problem expressed in terms of the modal amplitude functions $\phi_k(x)$. The solution of this problem consists of the member bifurcation pressure values (eigenvalues) and corresponding buckling mode shapes (eigenvectors). Such solution is obtained by means of a GBT-based beam finite element formulation similar to that recently developed and implemented by the authors (Basaglia *et al.* 2015, 2016)

3. Results and Discussion

Results concerning the elastic buckling behavior of several circular cylindrical steel tubes subjected to combination of axial compression and external lateral pressure are presented and discussed next. All tubes are simply supported, i.e., the end cross-sections are local and globally pinned and may warp freely. For validation purposes, some GBT-based critical buckling pressures and mode shapes are compared with values obtained by means of ANSYS shell finite element analyses (SAS 2013) – the cylindrical shells are discretized by means of refined meshes of SHELL181 elements, employed with a "full integration" option and accounting for distributed pressure follower effects. For cylinders/tubes under combined loading, the critical longitudinal stress (σ^c_{xx}) and pressure (p^c) components are given by

$$\sigma^c_{xx} = \lambda\cdot\alpha\cdot\sigma_{xx,cr} \qquad p^c = \lambda\cdot\beta\cdot p_{cr} \qquad \alpha+\beta=1 \quad , \quad (18)$$

where (i) λ is a load parameter (eigenvalue), (ii) α and β are compression-pressure parameters and (iii) $\sigma_{xx,cr}$ and p_{cr} are the member critical longitudinal stress and lateral pressure values when acted only by compression ($\alpha=1$ and $\beta=0$) and only by lateral pressure ($\alpha=0$ and $\beta=1$), respectively. By varying the values of parameters α and β between *0* and *1*, it is possible to determine a values of λ associated with any given load combination.

Initially, a few results concerning the buckling behavior of steel tubes acted by simple loadings (axial compression or lateral pressure) are presented and discussed, in order to provide a first illustration of the GBT analysis capabilities. Then, steel tubes under combinations of axial compression and lateral pressure are addressed, together with an investigation on the influence of the radius-to-thickness and length-to-radius ratios on the critical buckling loading and mode shape, carried out in the context of tubes with $r/t \le 100$ and *Z* parameter values covering a wide range, from small (≈*250*) to large (≈*215000*).

3.1 Tubes Subjected to Simple Loadings

Let us consider steel (Young's modulus $E=210GPa$ and Poisson's ration $\upsilon=0.3$) thin-walled tubes with wall thickness $t=0.12cm$, radius $r=6cm$ ($r/t=50$), $r=9cm$ ($r/t=75$) and $r=12cm$ ($r/t=100$), and subjected to either axial compression or lateral pressure. Figures 5 and 6 display the variations of the critical longitudinal stress ($\sigma_{xx,cr}$) or lateral pressure (p_{cr}) with the tube length L, respectively. Moreover, these figures also show (i) ANSYS 3D critical buckling loadings and mode shapes, and (ii) an indication of the GBT deformation modes contributing to the tube critical buckling modes (the values in brackets indicate the buckling mode longitudinal half-wave number). The observation of these buckling results prompts the following comments:

(i) The GBT and ANSYS critical buckling loadings are practically identical, as the differences never exceed *3.5%*. Moreover, there is also very close agreement between the buckling mode shapes provided by the two analyses.

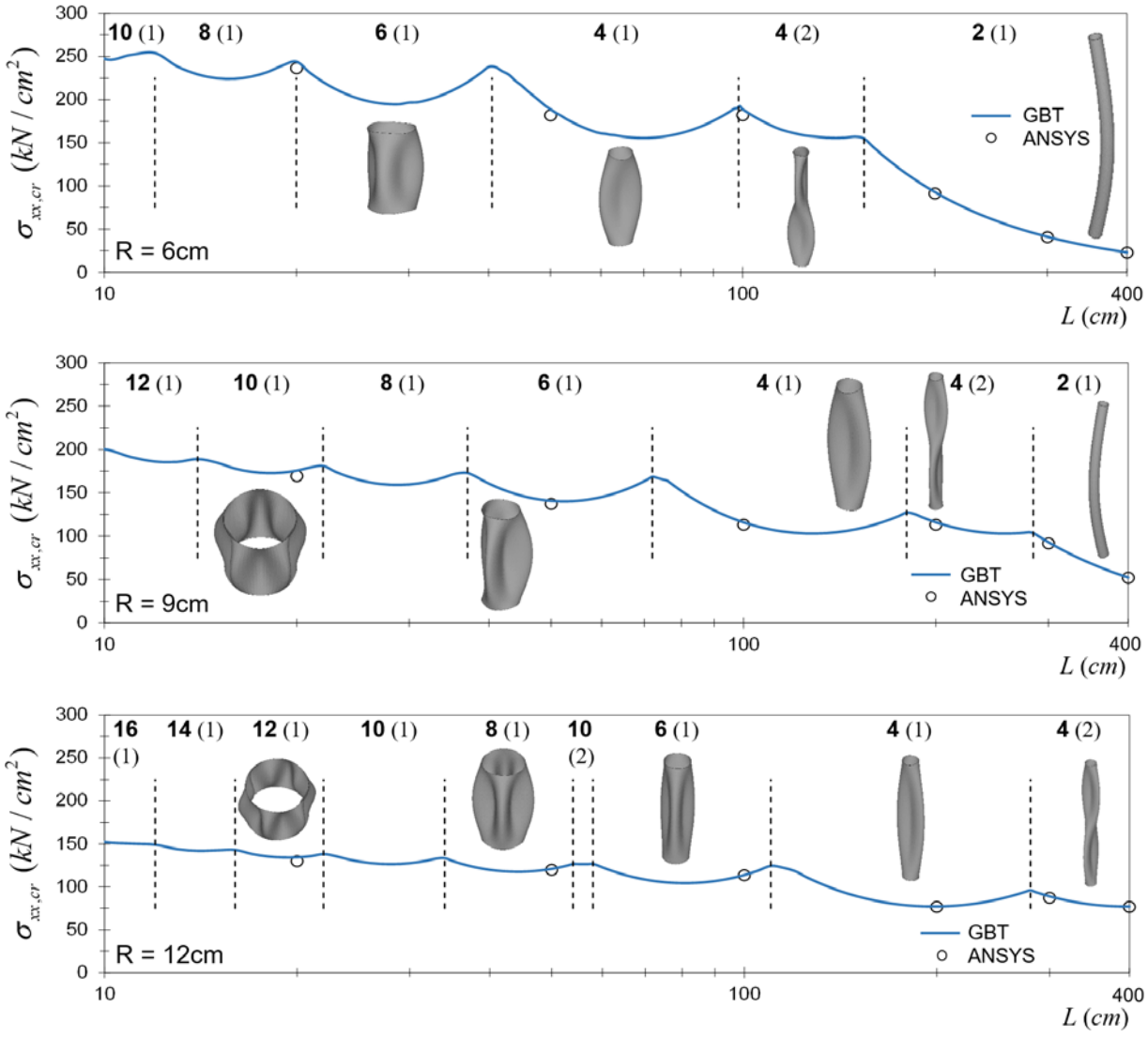

Figure 5: Variation of the critical longitudinal stress $\sigma_{xx,cr}$ and buckling mode shape with the tube length L.

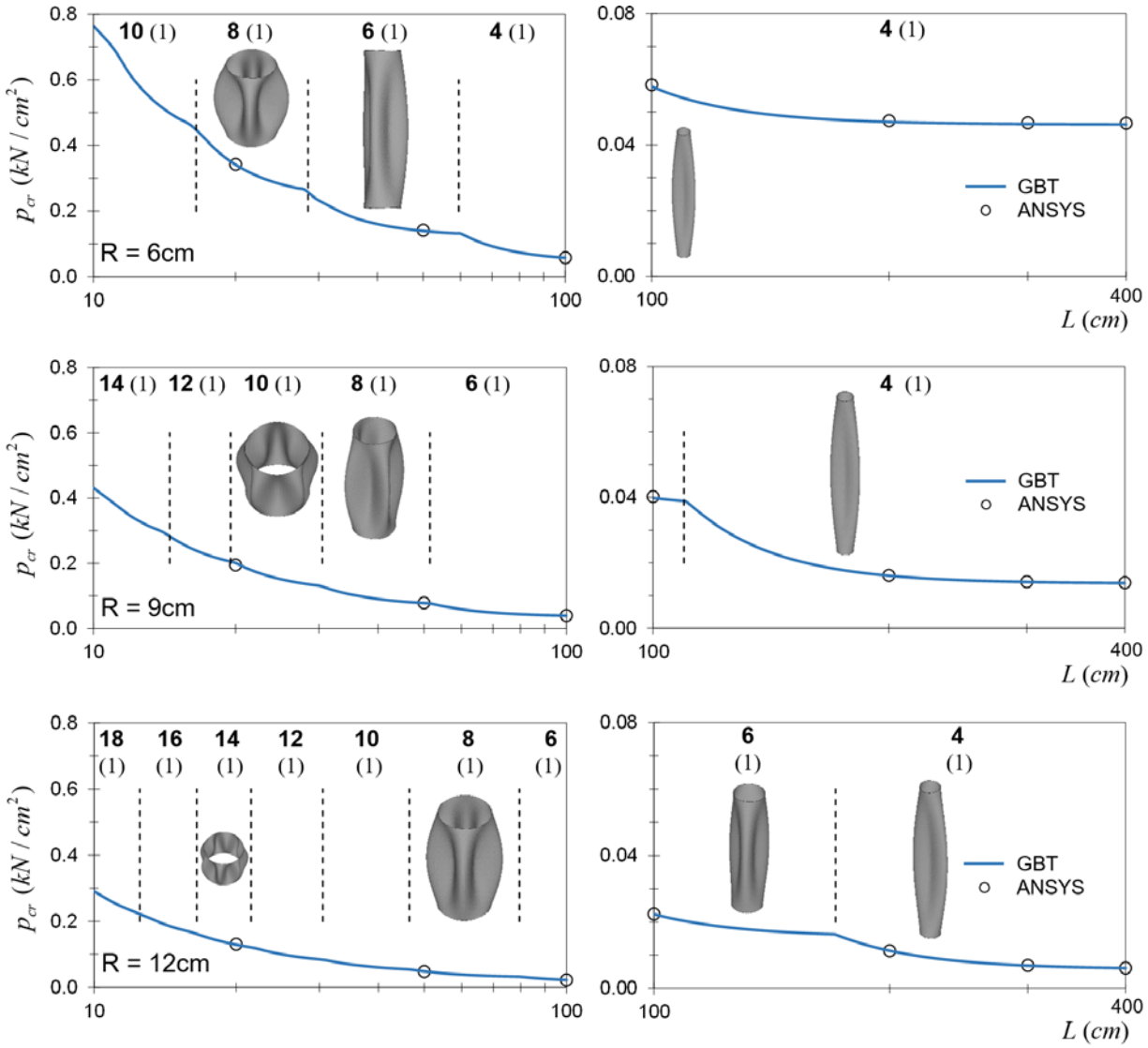

Figure 6: Variation of the critical lateral pressure p_{cr} and buckling mode shape with the tube length L.

(ii) In the compressed tubes, there is an expected visible critical load drop in the intermediate-to-long length range, which is associated with critical buckling in flexural modes (deformation mode **2**). In tubes under lateral pressure, on the other hand, a critical value drop occurs in the short-to-intermediate length range, associated with the critical buckling modes exhibiting *3* or more circumferential waves (*i.e.*, deformation modes **6** or higher – see Fig. 3). In both loading cases, the above critical value drops are more pronounced in the *r=6cm* tubes (*r/t=50*).

(iii) Between *L=20cm* and *L=400cm*, the tubes under lateral pressure buckle in critical modes exhibiting *2* to *7* circumferential waves (deformation modes **4** to **14** – see Fig. 3) and a single longitudinal half-wave – no critical buckling mode has a contribution from the flexural deformation mode **2**. Conversely, for the same length range the compressed tubes buckle in critical modes exhibiting up to *6* circumferential waves (deformation mode **12**) and two longitudinal half-waves – moreover, with the exception of the *r=12cm* tube, the flexural mode **2** always participates in the buckling mode.

(iv) Tubes with $r=6cm$ exhibit the same buckling mode shape under axial compression and lateral pressure for the following length intervals: (iv_1) $17cm \leq L \leq 19cm$ (deformation mode **8**), (iv_2) $29cm \leq L \leq 39cm$ (deformation mode **6**) and (iv_3) $60cm \leq L \leq 98cm$ (deformation mode **4** (1)). The same happens in tubes with $r=9cm$ and $r=12cm$. In the first case, for the length intervals (iv_1) $20cm \leq L \leq 21cm$ (deformation mode **10**), (iv_2) $31cm \leq L \leq 36cm$ (deformation mode **8**), (iv_3) $52cm \leq L \leq 71cm$ (deformation mode **6**) and (iv_4) $110cm \leq L \leq 180cm$ (deformation mode **4** (1)). In the second case, for the length intervals (iv_1) $31cm \leq L \leq 33cm$ (deformation mode **10**), (iv_2) $47cm \leq L \leq 54cm$ (deformation mode **8**), (iv_3) $80cm \leq L \leq 110cm$ (deformation mode **6**) and (iv_4) $171cm \leq L \leq 275cm$ (deformation mode **4** (1).

(v) In long tubes ($L>300cm$), as expected (recall the works of Iwata *et al.* 1991 and Basaglia *et al.* 2016), the critical pressure value is length-independent and corresponds to an ovalized buckling mode (deformation mode **4**).

3.2 Tubes Subjected to Combined Loadings

The tubes analyzed in this section exhibit the same cross-section dimensions, material properties and boundary conditions considered in the previous section, dealing with simple loadings. In order to cover wide Z parameter ($265 \leq Z \leq 211986$) and L/r ratio (of $1.67 \leq L/r \leq 66.67$) ranges, six tube lengths were selected: $L=20;50;100;200;300;400cm$. The GBT and ANSYS results are plotted in Figures 7 to 9, which make it possible to assess the critical buckling loadings of tubes with three radius values, namely $r/t=50;75;100$. The loadings consist of continuously varying combinations of axial compression and lateral pressure, and the figures exhibit plots $\sigma_{xx}^{c} / \sigma_{xx,cr}$ vs. p^{c} / p_{cr} – recall that (i) $\sigma_{xx,cr}$ and p_{cr} are the critical axial compression and external lateral pressure (acting alone), respectively, and (ii) σ_{xx}^{c} and p^{c} define the critical σ_{xx}-p combinations associated with combined loadings (see eq. (18)).

While the GBT analyses involve tube longitudinal discretizations in *8* beam finite elements and include *7* deformation modes (**2**+**4**+**6**+**8**+**10**+**12**+**14**), which amounts to a total of *112* degrees of freedom, the ANSYS SFE analyses involve tube discretizations into fairly refined meshes, which lead to degree of freedom numbers varying between *11088* ($L=20cm + r=12cm$) and *211728* ($L=400cm + r=12cm$). Although no special effort was made to minimize/optimize the shell finite element discretization, it is clear that the degree of freedom numbers involved in the two approaches are orders of magnitude apart. This difference is even more striking if one realizes that it is possible to include in the GBT analyses only a fairly small fraction (appropriately selected, of course) of the deformation modes determined.

The analysis of the GBT and ANSYS buckling results presented leads to the following remarks:

(i) Once again, the GBT and ANSYS critical loadings are very close (differences below not *3.7%*) and there is an excellent agreement between the corresponding buckling mode shapes.

(ii) The interaction diagrams, providing critical combinations of axial compression and lateral pressure, are either linear or multi-linear – in the latter case, all of them exhibit a "convex shape"[6].

(iii) In the multi-linear interaction diagrams, the transition points between linear segments are associated with sudden changes in the tube critical buckling mode shape. It should be mentioned that the most pronounced transitions occur in the longer tubes ($L=200;300;400cm$) and correspond to either (iii_1) critical buckling modes changes from flexural (deformation mode **2**) to ovalized (deformation mode **4**) or (iii_2) decreases in the critical buckling mode longitudinal half-wave number.

[6] Since all the tubes analyzed are such that $Z>20$, no interaction diagram exhibits a "concave shape", like those reported by Tennyson *et al.* (1978).

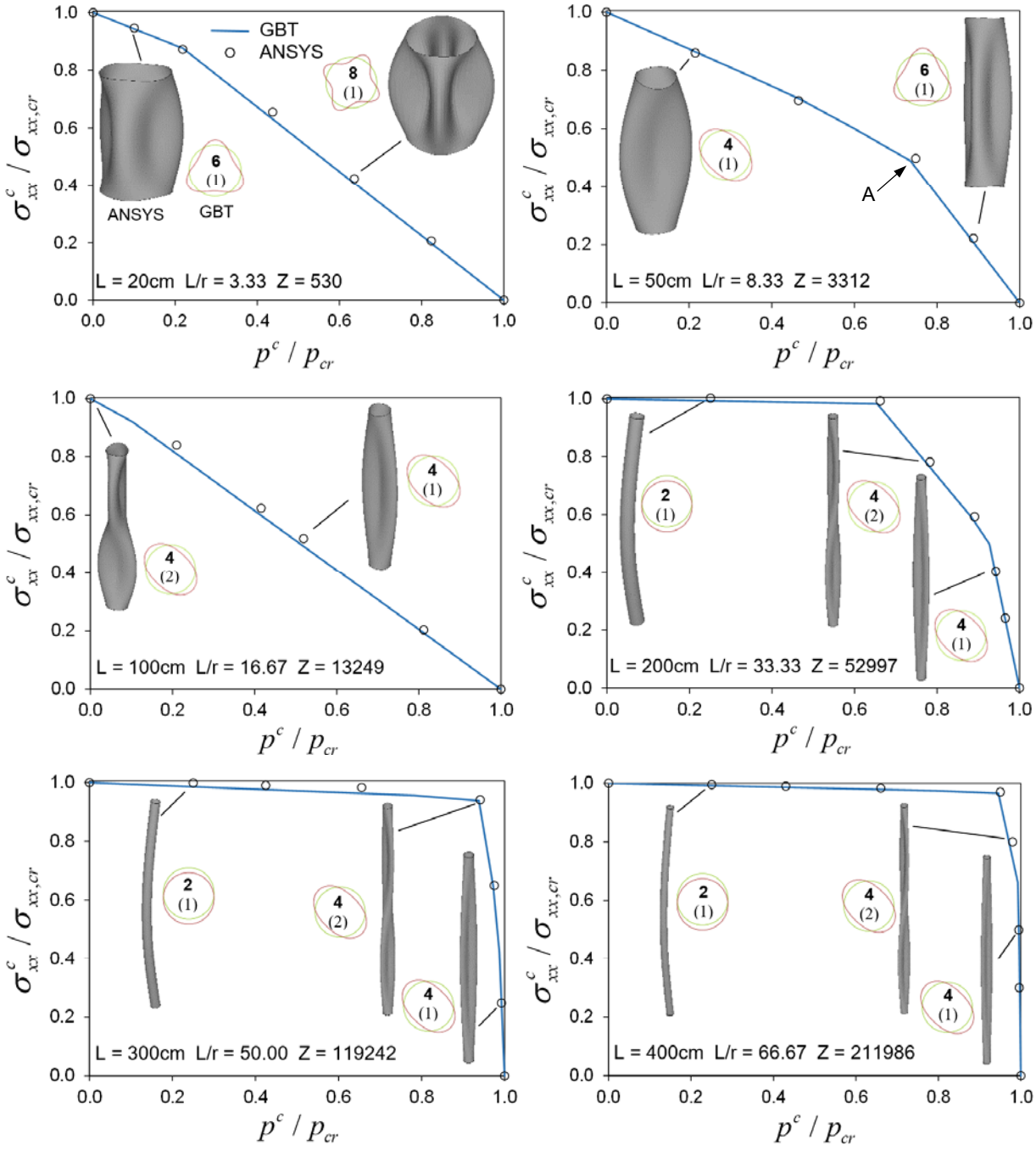

Figure 7: GBT and ANSYS critical combined loadings and buckling modes for $r=6\,cm$ tubes.

(iv) The interaction diagram is linear in the tubes with (iv$_1$) $L=20\,cm$, for $r=9\,cm$ and (iv$_2$) $L=50$;100;$200\,cm$, for $r=12\,cm$ – the observation of Figures 5 and 6 shows that these tubes exhibit identical buckling modes under axial compression and lateral pressure: deformation mode **10**, for $L=20\,cm$, $r=9\,cm$, deformation mode **8**, for $L=50\,cm$, $r=12\,cm$, deformation mode **6**, for $L=100\,cm$, $r=12\,cm$, and deformation mode **4**, for $L=200\,cm$, $r=12\,cm$. It is worth noting that, for very thin shells, a linear interaction diagram is prescribed in EN 1993-1-6:2007 (CEN 2007) – linear interaction diagrams were also proposed in the NASA-SP-8007 (1968) report.

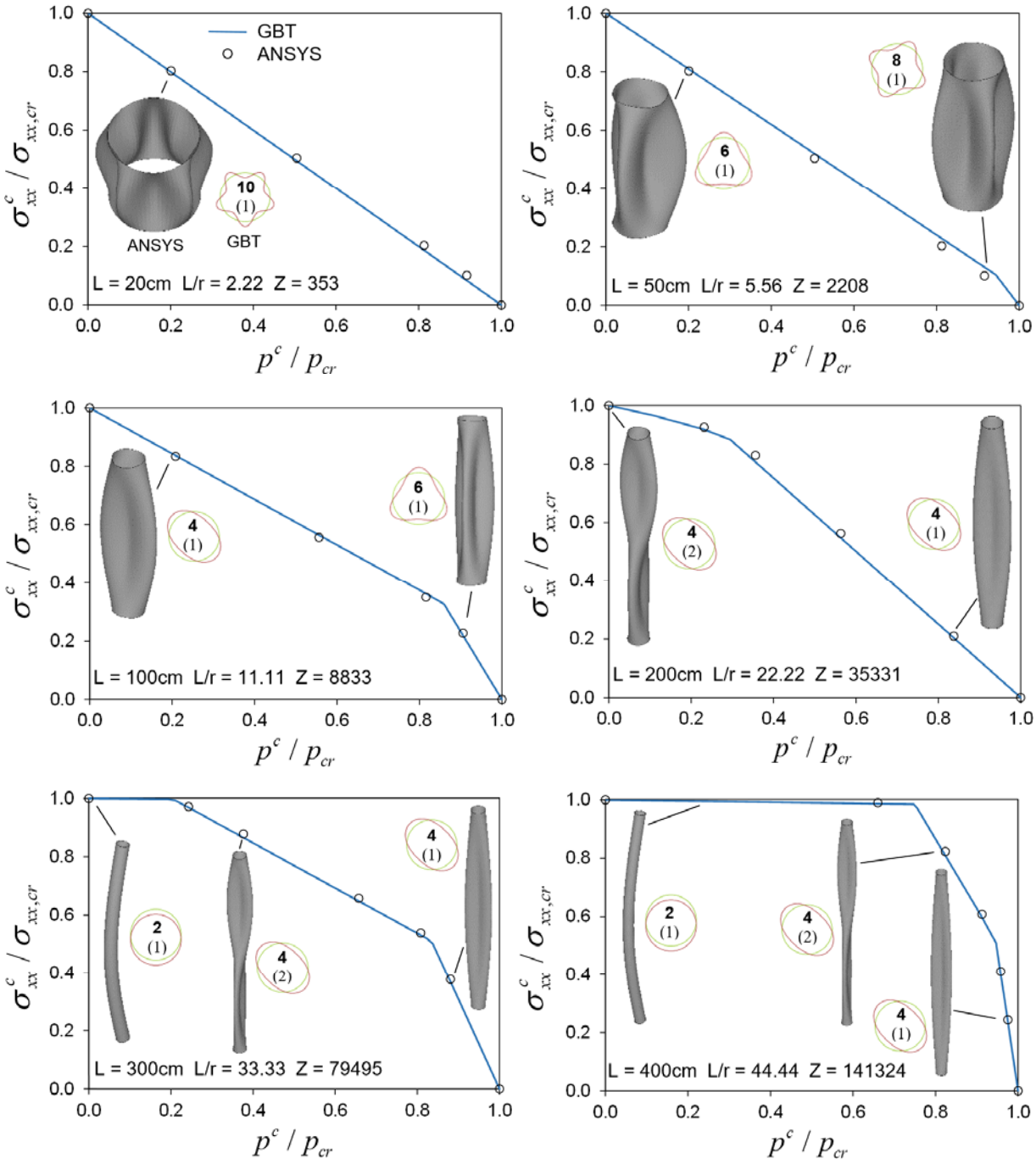

Figure 8: GBT and ANSYS critical combined loadings and buckling modes for $r=9\,cm$ tubes.

(v) However, the code and report mentioned in the previous item pay no attention to tubes for which the critical buckling mode shapes under axial compression and external lateral pressure differ – these tubes are addressed ahead in the paper.

(vi) In the longer tubes, with $L/R>40$ and $Z>100000$ (*i.e.*, $L=300$ or $400cm$ and $r=6cm$, or $L=400cm$ and $r=9cm$ – see Figs. 7 and 8), the buckling behavior is governed by axial compression, associated with flexural critical buckling modes (deformation mode **2**) and the influence of the external lateral

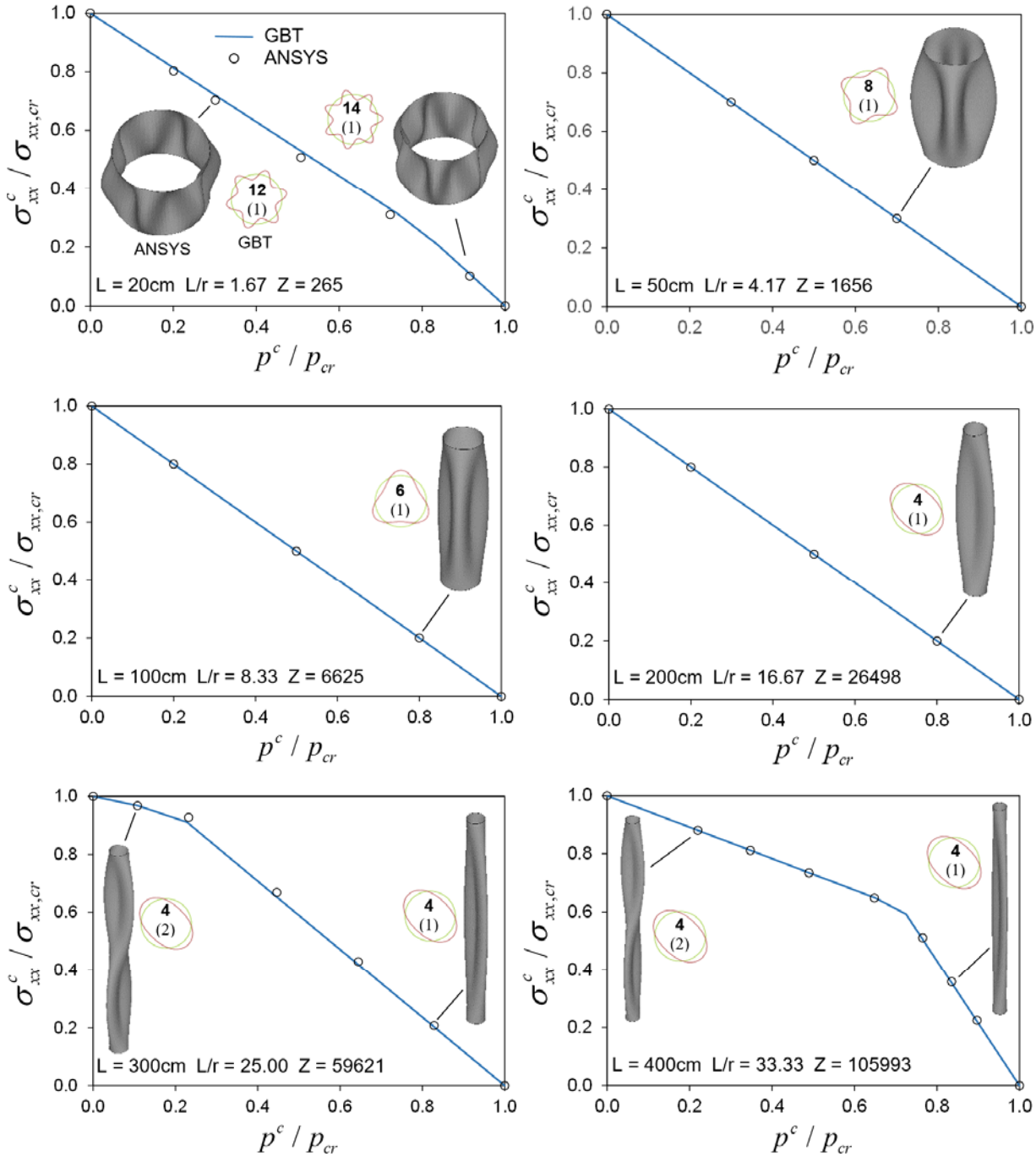

Figure 9: GBT and ANSYS critical combined loadings and buckling modes for $r=12\,cm$ tubes.

pressure is minute up to very large fractions of p_{cr} – note the "almost horizontal" line segments in the last two plots of Figure 7 and the last plot of Figure 8.

(vii) The sole use of parameter Z to classify the tubes and to assess the curvature effects on their buckling behavior is clearly inadequate. This assertion can be confirmed by looking at Figure 10, which display the interaction diagrams of tubes with (i) $r=6\,cm$, $t=0.12\,cm$ and $L=203.7\,cm$, (ii) $r=9\,cm$, $t=0.12\,cm$ and $L=249.5\,cm$, and (iii) $r=12\,cm$, $t=0.12\,cm$ and $L=288.1\,cm$, all three sharing the same

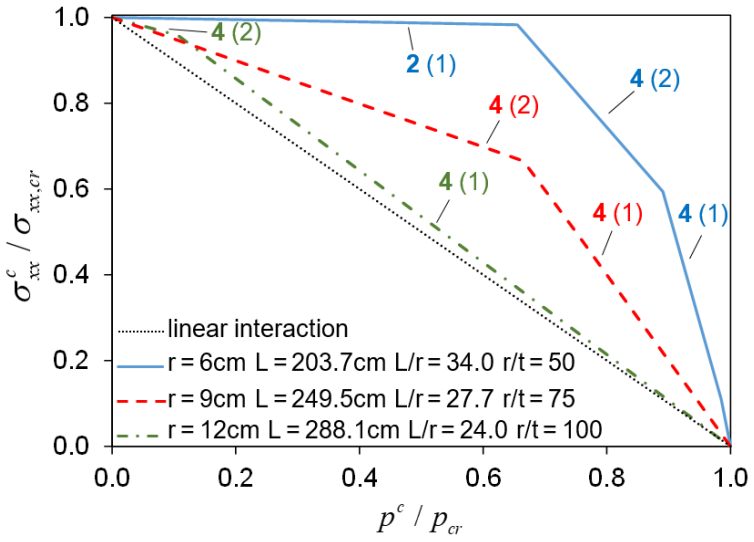

Figure 10: Critical combined loadings for tubes with *Z=55000*.

parameter *Z* value (*Z=55000*) – also shown is the linear interaction diagram. Note that none of the three interaction diagrams is linear – while those concerning the *r=12cm* and *r=9cm* tubes are bi-linear, the one related to the *r=6cm* tube is tri-linear. Moreover, it is also clear that these interaction diagrams "move away" from the linear one (*i.e.*, become "more convex") as the tube radius decreases – indeed, while the *r=12cm* tube bi-linear interaction diagram is "almost linear", the *r=6cm* tube tri-linear interaction diagram is "substantially convex".

4. Conclusion

This paper presented and discussed the available results of an ongoing numerical investigation on the buckling behavior of thin-walled steel tubes subjected to combinations of axial compression and external lateral pressure. These results were obtained by means of a beam finite element implementation of a computationally efficient GBT formulation specifically developed for circular cylindrical shells and tubes, and making it possible to solve a large number of problems in a very short period of time – for validation purposes, some GBT results were compared with values obtained by means of ANSYS shell finite element analyses. After providing a brief overview of the main concepts and procedures involved in performing GBT buckling analyses, numerical illustrative examples were presented and discussed. Initially, a few results concerning the buckling behaviour of steel tubes acted by simple loadings (only axial compression or external lateral pressure) were addressed. Then, a limited parametric study was performed for steel tubes under various combined loadings, consisting of combinations of axial compression and external lateral pressure – this parametric study also aimed at investigating the influence of the radius-to-thickness and length-to-radius ratios on the critical buckling loading and mode shape, in the context of tubes with $r / t \leq 100$ and *Z* parameter values varying between *≈250* and *≈215000*. The results obtained demonstrated that the sole use of parameter *Z* to classify tubes and assess the curvature effects on their buckling behavior is inadequate. Moreover, it was also clearly shown that adopting a linear interaction diagram to predict the critical buckling loading of tubes subjected to combinations of axial compression and external lateral pressure, as has been proposed in the literature and is still prescribed by the current European code (CEN 2007), may lead to very conservative estimates, particularly for tubes exhibiting large length-to-radius ratios. Further research is needed in order to achieve a more efficient (less conservative) critical buckling loading prediction.

Acknowledgments

The first author acknowledges the financial support provided by *Conselho Nacional de Desenvolvimento Científico e Tecnológico* (CNPq – Ministry of Science, Technology and Innovation of Brazil), through project 308530/2016-0

References

Arjomandi K (2010). *Mechanical Response of Sandwich Pipes Subject to Hydrostatic Pressure and Bending*, Ph.D. Thesis, Department of Civil and Resource Engineering, Dalhousie University, Halifax, Canada.

Basaglia C, Camotim D, Silvestre N (2015). Buckling and vibration analysis of cold-formed steel CHS members and frames using generalized beam theory, *International Journal of Structural Stability and Dynamics*, **15**(8), 1540021-1 - 1540021-25.

Basaglia C, Camotim D, Silvestre N, Palermo Jr. L (2016). GBT-based buckling analysis of circular cylindrical steel shells under uniform external pressure, *Website Proceedings of SSRC Annual Stability Conference* (Orlando, 12-15/4).

Batdorf SB (1947). *A Simplified Method of Elastic-Stability Analysis for Thin Cylindrical Shells II – Modified Equilibirium Equation*, National Advisory Committee for Aeronautics (NACA) Report No. 1342, 1-33.

CEN (Comité Européen de Normalisation) (2007). – *Eurocode 3: Design of Steel Structures – Part 1.6: Strength and Stability of Shell Structures*, EN 1993-1-6:2007, Brussels, Belgium.

Galletly GD, Pemsing K (1985). Interactive buckling tests on cylindrical shells subjected to axial compression and external pressure – a comparison of experiment, theory and various codes, *Proceedings of the Institution of Mechanical Engineers, Part C: Journal of Mechanical Engineering Science*, **199**(4), 259-280.

Iwata K, Tsukimori K, Kubo F (1991). A symmetric load-stiffness matrix for buckling analysis, *International Journal of Pressure Vessels and Piping*, **45**(1), 101-120.

Krishnamoorthy G (1974). Buckling of thin cylinder under combined external pressure and axial compression, *Journal of Aircraft*, **11**(2), 65-68.

Kyriakides S, Corona E (2007). *Mechanics of Offshore Pipelines – Vol. 1: Buckling and Collapse*, Elsevier, Oxford.

NASA (National Aeronautics and Space Administration) (1968). *Buckling of Thin Walled Circular Cylinders*, Report No SP-8007, NASA Space Vehicle Design Criteria (Structures), Springfield, Virginia.

Paimushin VN (2008). Static and dynamic beam forms of the loss of stability of a long orthotropic cylindrical shell under external pressure, *Journal of Applied Mathematics and Mechanics*, **72**(6), 738-747.

Ross CTF (2011). *Pressure Vessels: External Pressure Technology* (2nd edition), Woodhead Publishing Limited, Cambridge.

SAS (Swanson Analysis Systems Inc.) (2013). *ANSYS Reference Manual* (version 15).

Schardt R (1989). *Verallgemeinerte Technishe Biegetheorie*, Springer-Verlag (Berlin). (German)

Shen H-S, Chen T-Y (1991). Buckling and postbuckling behaviour of cylindrical shells under combined external pressure and axial compression, *Thin-Walled Structures*, **12**(4), 321-334.

Silvestre N (2007). Generalised beam theory to analyse the buckling behaviour of circular cylindrical shells and tubes, *Thin-Walled Structures*, **45**(2) 185-198.

Sun J, Xu X, Lim CW (2016). Combined load buckling for cylindrical shells based on a symplectic elasticity approach, *Journal of Theoretical and Applied Mechanics*, **54**(3), 705-716.

Teng JG, Rotter JM (2004). Buckling of thin shells: an overview, *Buckling of Thin Metal Shells*, J.G. Teng & J.M. Rotter (eds.), Spon Press, London, 1-41.

Tennyson RC, Booton M, Chan KH (1978). Buckling of short cylinders under combined loading, *Journal of Applied Mechanics* (ASME), **3**(5), 913-920.

Weingarten VI, Seide P (1965). Elastic stability of thin-walled cylindrical and conical shells under combined external pressure and axial compression, *American Institute of Aeronautics and Astronautics* (*AIAA*) *Journal*, **3**(5), 913-920.

Winterstetter TA, Schmidt H (2002). Stability of circular cylindrical steel shells under combined loading, *Thin-Walled Structures*, **40**(10), 893-910.

Yamaki N (1984). *Elastic Stability of Circular Cylindrical Shells*, North-Holland Series in Applied Mathematics and Mechanics, Vol. 27, Elsevier, Amsterdam.